THE JOURNAL OF BIOLOGICAL CHEMISTRY VOL. 287, NO. 8, pp. 5698–5709, February 17, 2012


# Structure of Minimal Tetratricopeptide Repeat Domain Protein Tah1 Reveals Mechanism of Its Interaction with Pih1 and Hsp90*[S]

Received for publication, July 28, 2011, and in revised form, December 5, 2011 Published, JBC Papers in Press, December 16, 2011, DOI 10.1074/jbc.M111.287458

**Beatriz Jiménez**[‡1,2,3], **Francisca Ugwu**[§1,4], **Rongmin Zhao**[¶], **Leticia Ortí**[‡], **Taras Makhnevych**[§], **Antonio Pineda-Lucena**[‡3,5], **and Walid A. Houry**[§6]

*From the* [‡]*Structural Biochemistry Laboratory, Medicinal Chemistry Department, Centro de Investigación Príncipe Felipe, E-46012 Valencia, Spain, the* [§]*Department of Biochemistry, University of Toronto, Toronto, Ontario M5S 1A8, Canada, and the* [¶]*Department of Biological Sciences, University of Toronto Scarborough, Scarborough, Ontario M1C 1A4, Canada*

**Background:** Tah1 and Pih1 are Hsp90 interactors that form a ternary complex with the chaperone.
**Results:** NMR structure of Tah1 revealed the presence of two tetratricopeptide repeat motifs followed by a C helix and an unstructured region.
**Conclusion:** Tah1 can bind simultaneously two other proteins using different interaction modes.
**Significance:** The study provides important insights into protein complex assembly.

**Tah1 and Pih1 are novel Hsp90 interactors. Tah1 acts as a cofactor of Hsp90 to stabilize Pih1. In yeast, Hsp90, Tah1, and Pih1 were found to form a complex that is required for ribosomal RNA processing through their effect on box C/D small nucleolar ribonucleoprotein assembly. Tah1 is a minimal tetratricopeptide repeat protein of 111 amino acid residues that binds to the C terminus of the Hsp90 molecular chaperone, whereas Pih1 consists of 344 residues of unknown fold. The NMR structure of Tah1 has been solved, and this structure shows the presence of two tetratricopeptide repeat motifs followed by a C helix and an unstructured region. The binding of Tah1 to Hsp90 is mediated by the EEVD C-terminal residues of Hsp90, which bind to a positively charged channel formed by Tah1. Five highly conserved residues, which form a two-carboxylate clamp that tightly interacts with the ultimate Asp-0 residue of the bound peptide, are also present in Tah1. Tah1 was found to bind to the C terminus of Pih1 through the C helix and the unstructured region. The C terminus of Pih1 destabilizes the protein *in vitro* and *in vivo*, whereas the binding of Tah1 to Pih1 allows for the formation of a stable complex. Based on our data, a model for an Hsp90-Tah1-Pih1 ternary complex is proposed.**

Tah1 (TPR[7]-containing protein associated with Hsp90) is a small protein of 111 amino acids (12.5 kDa). We discovered this previously uncharacterized protein during a proteomic screen for Hsp90 interactors (1). We demonstrated that Tah1 is a novel Hsp90 cofactor that modulates the chaperone activity. Tah1 was found to interact with Hsp90 as well as with another protein that we termed Pih1 (also called Nop17; 344 residues) (1). Hsp90-Tah1 function to stabilize Pih1 and to promote the formation of an Rvb1-Rvb2-Tah1-Pih1 complex, which we named the R2TP complex (2). Rvb1 and Rvb2 are two highly conserved AAA+ helicases involved in many different critical complexes in the cell (3, 4). The R2TP complex is highly conserved from yeast to mammalian cells and has been shown to be required for the proper assembly of box C/D small nucleolar ribonucleoproteins (5, 2), for the assembly of RNA polymerase II (6, 7), and for the stability of the phosphatidylinositol 3-kinase-related kinases through binding to TEL2 (8). Furthermore, both human Pih1 (PIH1D1) and human Tah1 (RPAP3) have been shown to regulate apoptosis (9, 10).

A TPR motif typically consists of 34 amino acids that adopt a helix-turn-helix structure. The motif is defined by a pattern of small and large hydrophobic amino acids, with no positions being completely invariant. The motif was initially discovered in cell cycle regulatory proteins Cdc23 and Nuc2 (11, 12). Most TPR proteins contain between 3 and 16 TPR repeats (13, 14), with adjacent TPR motifs packed in a parallel fashion, resulting in a spiral of $\alpha$-helices forming a right-handed superhelical arrangement that is typically capped by a C-terminal hydrophilic helix. As a result, a concave and a convex ligand binding interface are formed, making TPR proteins ideal for mediating protein-protein interactions and for acting as scaffolds for the assembly of multiprotein complexes (15, 16). TPR proteins have been implicated in a wide range of cellular activities, such

* This work was supported by a grant from the Canadian Institutes of Health Research (MOP-93778) to WAH, Spanish Ministerio de Ciencia e Innovación (MICINN, SAF2008-01845) to AP-L.
[S] This article contains supplemental Figs. 1 and 2.
*The atomic coordinates and structure factors (code 2L6J) have been deposited in the Protein Data Bank, Research Collaboratory for Structural Bioinformatics, Rutgers University, New Brunswick, NJ (http://www.rcsb.org/).*
[1] Both authors contributed equally to this work.
[2] A Sara Borrell fellow from the ISCIII (Spanish Ministry of Science and Innovation).
[3] Supported by the Access to Research Infrastructures activity in the 6th FP of the EC (Contract RII3-026145, EU-NMR).
[4] Supported in part by the Ontario Institute for Cancer Research and by the Grant Miller Cancer Research Grant from the Faculty of Medicine at the University of Toronto.
[5] To whom correspondence may be addressed. E-mail: apineda@cipf.es.
[6] To whom correspondence may be addressed. E-mail: walid.houry@utoronto.ca.

[7] The abbreviations used are: TPR, tetratricopeptide repeat; ITC, isothermal titration calorimetry; VHL, von Hippel-Lindau; HSQC, heteronuclear single quantum coherence.

as cell cycle regulation, transcriptional control, protein transport, and protein folding (17, 18).

Several TPR proteins are known to bind the C termini of the Hsp70 and Hsp90 chaperones and to act as cofactors that modulate the function of these chaperones (19, 20). Several groups have reported the crystal structures of TPR domains in complex with peptides that include the C-terminal EEVD residues of Hsp90 and Hsp70 (21–24, 16). These structures provide insights into the molecular basis of TPR-ligand recognition. Typically, the TPR domains in these structures consist of three TPR motifs and a C-terminal cap helix (see below). In this regard, Tah1 is rather unusual because, based on secondary structure analysis programs, it has only two predicted TPR motifs but can still interact with Hsp90 (1, 2). We had demonstrated that Tah1 interaction with Hsp90 is mediated by the C terminus of the chaperone (2). We also showed that the C-terminal fragment of Tah1, consisting of residues 76–111, can bind to Pih1 (2).

In order to understand the basis by which this minimal TPR domain protein attains a folded and stable structure and how it interacts with Pih1 and Hsp90, the NMR structure of Tah1 was solved, and its interaction with Pih1 and Hsp90 was investigated. Our findings show that Tah1 is a stable two-TPR repeat protein with a C-terminal cap helix and an unstructured region. Tah1 forms a positively charged channel in which the MEEVD model peptide binds. Furthermore, the C terminus of Tah1 was found to bind to the C terminus of Pih1. Biochemical and biophysical studies suggest a model of the Hsp90-Tah1-Pih1 ternary complex.

## EXPERIMENTAL PROCEDURES

*Plasmid Construction*—The construction, expression, and purification of full-length Tah1 and Pih1 have been described previously (2). Pih1(1–230), Pih1(1–284), Pih1(231–344), Tah1(1–74), and Tah1(1–93) were amplified from yeast *Saccharomyces cerevisiae* S288C genome, cloned into p11 expression vector (25), and expressed with an N-terminal $His_6$ tag followed by tobacco etch virus protease cleavage site. To make Pih1-Tah1, Pih1-Tah1(75–111), and Pih1-Tah1(94–111) fusion constructs, the Pih1 coding sequence was amplified using forward and reverse primers carrying an NdeI and a HindIII site, respectively. The Tah1, Tah1(75–111), and Tah1(94–111) were amplified using primers carrying HindIII and BamHI sites. The NdeI-HindIII Pih1 coding sequence was then ligated together with the HindIII-BamHI Tah1 coding sequence constructs and inserted into the NdeI/BamHI sites in p11.

Site-directed mutagenesis was carried out following protocols described in the Stratagene QuikChange site-directed mutagenesis kit instruction manual (Stratagene, La Jolla, CA). Each mutation was confirmed by DNA sequencing.

*Protein Purification*—All $His_6$-tagged proteins were expressed in *E. coli* BL21(DE3) gold (pRIL) and purified using $Ni^{2+}$-NTA resin (Qiagen) according to the manufacturer's protocols. For labeled samples required for NMR measurements, cells were grown in M9 medium supplemented with $[^{15}N]NH_4Cl$ and/or $[^{13}C]$glucose as nitrogen and carbon sources, respectively. The purified proteins were typically dialyzed and stored in buffer A (25 mM Tris-HCl, pH 7.5, 100 mM KCl, 10% glycerol, and 1 mM DTT). Tobacco etch virus (TEV) protease was used to remove the $His_6$ tag. The concentrations of purified proteins were determined using the Bradford assay (26).

*Size Exclusion Chromatography*—Size exclusion chromatography was performed using a calibrated Superdex 200 or 75 HR 10/30 column (GE Healthcare) attached to an AKTA FPLC system (GE Healthcare). The column was equilibrated with buffer B (25 mM Tris-HCl, pH 7.5, 100 mM KCl, 10% glycerol, and 1 mM DTT). To test the oligomeric state of the purified proteins, at least 500 $\mu$g of protein in a total volume of 500 $\mu$l were loaded onto Superdex 200. To test the interaction between Tah1/Tah1 fragments with Pih1/Pih1 fragments, 250 $\mu$g of each protein were mixed in a total volume of 250 $\mu$l and loaded onto Superdex 75. Where indicated, WT Tah1 was preincubated with 450 $\mu$M of MEEVD peptide overnight at 4 °C prior to the addition of Pih1. Molecular weight standards used were purchased from Sigma or Bio-Rad: thryoglobulin (669 kDa), apoferritin (443 kDa), $\alpha$-amylase (200 kDa), alcohol dehydrogenase (150 kDa), bovine serum albumin (66 kDa), ovalbumin (44 kDa), carbonic anhydrase (29 kDa), myoglobin (17 kDa), cytochrome *c* (12.4 kDa), aprotinin (6.5 kDa), and vitamin $B_{12}$ (1.4 kDa). All experiments were performed at 4 °C, and absorbance was monitored at 280 nm.

*Isothermal Titration Calorimetry*—Purified Tah1 and its mutants were dialyzed overnight at 4 °C in buffer C (20 mM Tris-HCl, pH 8.0, 1 mM EDTA, and 5 mM NaCl). Protein concentrations were determined by absorbance at 280 nm using an ND-1000 Spectrophotometer (Thermo Scientific). The MEEVD peptide (663.7 daltons), containing an acetyl moiety at the N terminus and a free C-terminal carboxylate group, was synthesized at the Synthesis of Peptide Service at the Centro de Investigación Príncipe Felipe (Valencia, Spain) using a 433A Applied Biosystems synthesizer and Fmoc (*N*-(9-fluorenyl)methoxycarbonyl) chemistry. The peptide was weighed on an analytical balance (Mettler) and dissolved in buffer C. Samples were filtered using a 0.45-$\mu$m pore syringe filter (Pall Life Sciences) and degassed.

Isothermal Titration Calorimetry (ITC) measurements were performed at 4 °C in buffer C using a VP-ITC microcalorimeter (Microcal) with a cell volume of 1.458 ml. Peptide concentration in the needle was 450 $\mu$M, and Tah1 concentration in the cell was 30 $\mu$M. The syringe speed was set at 310 rpm, and a 150-s delay time was maintained between each injection. Heat of dilution was determined in a separate experiment by injecting peptide into buffer in the same sequence. The enthalpy value of the first injection was omitted due to experimental errors, and thermodynamic parameters were derived using a non-linear least square curve-fitting algorithm (Microcal Origin) to an *n*-identical independent binding model with three variables: association constant ($K_b$), enthalpy ($\Delta H$), and stoichiometry ($n$). Other thermodynamic parameters and their S.D. values, namely dissociation constant ($K_d$), Gibbs free energy ($\Delta G$), and entropy ($\Delta S$), were derived from $K_b$ and $\Delta H$.

*NMR Experiments*—Purified proteins were dialyzed in buffer D (25 mM $NaH_2PO_4/Na_2HPO_4$, pH 8, and 100 mM NaCl) and concentrated to a final concentration between 400 $\mu$M and 1 mM, depending on the NMR experiment. 10% $D_2O$ was present in the final solution. All two- and three-dimensional NMR

experiments were acquired at 293 K using Bruker Avance II spectrometers equipped with a TCI cryoprobe and working at 600.13 or 899.58 MHz for $^{1}$H. Tah1-MEEVD backbone assignment was achieved using a set of three-dimensional experiments based on *J* couplings: HNCO, HNCA, HNCACB, CBCACONH, and HBHACONH. Side chain assignments were based on the analysis of hCCH-TOCSY and HcCH-TOCSY experiments together with $^{1}$H,$^{15}$N-NOESY-HSQC, aliphatic $^{1}$H,$^{13}$C-NOESY-HSQC, and aromatic $^{1}$H,$^{13}$C-NOESY-HSQC. Additionally, $^{13}$C direct detection experiments CC-COSY and CACO were used for the assignment of Asx and Glx residue side chains. Upper distance limit constraints were calculated from two-dimensional $^{1}$H,$^{1}$H NOESY, two-dimensional $^{15}$N-filtered $^{1}$H,$^{1}$H NOESY, three-dimensional $^{1}$H,$^{13}$C NOESY-HSQC, and $^{1}$H,$^{15}$N NOESY-HSQC. Spectral windows of 12 ppm for $^{1}$H, 28 ppm for $^{15}$N, and 16 ppm (HNCO), 30 ppm (HNCA), or 62 ppm (CBCA(CO)NH) for $^{13}$C were used with their center set at 4.7, 115, 175, 53, and 39 ppm, respectively. The relaxation delay used was 1.1 s, and 8–32 scans were collected. The $^{13}$C direct detection experiments were acquired with 60 scans, relaxation delays of 1.4 s, and acquisition times of 72 ms. NMR spectra were acquired and processed using TOPSPIN (version 2.1, Bruker BioSpin, Rheinstetten, Germany) and analyzed using CARA software (ETH, Zurich, Switzerland). Two-dimensional $^{1}$H,$^{15}$N HSQC experiments were used to follow the binding of Tah1 to MEEVD peptide. $^{15}$N-labeled Tah1 was concentrated to 0.6 mM, and the peptide was titrated to a final concentration of 0, 0.3, 0.6, 0.89, 1.17, 1.7, and 2.2 mM. Chemical shift changes for the combined $^{1}$H and $^{15}$N nuclei ($\Delta\delta_{avg}^{HN}$) and signal broadening were used to map the interactions with peptide.

*Structure Calculations*—Assignment of the NOESY spectrum of Tah1 was performed using the algorithm ATNOS-CANDID integrated in the UNIO routine (27). Manual modifications were performed after inspection of the results. TALOS software (28) was used to calculate angle restraints derived from the chemical shifts in addition to the constraints already calculated by the UNIO routine. Hydrogen bond constraints were also obtained by solvent exchange and adequately introduced into the structure calculations. HADDOCK (29) was used to model the interaction between Tah1 and MEEVD using the data from NMR titrations, single point mutagenesis, and the solvent accessibility surfaces. Intermolecular NOEs were obtained from the $^{15}$N-edited two-dimensional NOESY and introduced into the structure calculations (supplemental Fig. 1). 500 random structures were minimized in the simulated annealing procedure using CYANA 2.1 (27), and the 20 conformers with lowest energy were selected. A summary of the constraints utilized can be found in Table 1. Energy minimization of this family of structures was performed using AMBER 10.0 in a water box of 10 Å (30) and the AMPS-NMR portal within the WeNMR gateway (available on the World Wide Web), which includes a molecular dynamics step for the structure minimization. Evaluation of the structure was done using PSVS (31) and CING (available on the World Wide Web). Validation outcome is summarized in Table 2. The protein secondary structure was assigned using TALOS (28). The full resonance assignment of the complex has been deposited in the BMRB data base with entry number 17312.

*Confocal Microscopy and in Vivo Analysis of Pih1 Stability*—pAG415GPD-EGFP-Pih1 plasmid was constructed using Pih1 ORF obtained from the Yeast FLEXGene collection (32). Pih1 ORF was first subcloned into Gateway® donor vector pDONR201 and then subcloned into the EGFP fusion expression vector pAG415GPD-EGFP following a published protocol (33). The plasmids p416ADH-GFP and p416ADH-GFP-Pih1(282–344) were constructed by amplifying the relevant Pih1 fragment from pET22-Pih1 (2) and GFP from pRSET-S65T (Clontech) and then ligating the fragments into the yeast expression vector p416ADH (34). pChFP-VHL was a gift from Dr. Judith Frydman (Stanford University).

S288C WT cells and *rpt6-25* mutant cells (a gift from Dr. Charles Boone, University of Toronto) transformed with either EGFP-Pih1 or GFP-Pih1(282–344) were grown in appropriate synthetic media to $A_{600}$ of 0.5 at room temperature, and then the temperature was shifted to 37 °C. At the indicated time points, cultures were pelleted, and a 1.5-$\mu$l suspension was spotted onto a glass slide for image analysis. Images were captured using the Quorum WaveFX Spinning Disc Confocal System.

To test the stability of GFP and GFP fusion proteins *in vivo*, the plasmids p416ADH-GFP and p416ADH-GFP-Pih1(282–344) were transformed into yeast strain W303. The cells were grown to midlog phase, and then cycloheximide was added to the culture at a final concentration of 50 $\mu$g/ml. Equal volumes of cell cultures were then withdrawn at different time points and lysed. Proteins were separated on 12% SDS-polyacrylamide gels, followed by immunoblotting using anti-GFP antibody (G1544, Sigma).

## RESULTS

*NMR Structure of Tah1-MEEVD*—Initial attempts to determine the NMR structure of free Tah1 were unsuccessful because the protein was not stable long enough at the concentrations needed for the heteronuclear NMR experiments. The addition of MEEVD, resembling the C-terminal residues of Hsp90/Hsp70, stabilized the protein and allowed the determination of the solution NMR structure of Tah1 in complex with the peptide (see "Experimental Procedures"). Such instability of apo-TPR domains has been observed before for other proteins, such as for protein phosphatase 5 (35). The MEEVD peptide used in our studies was acetylated at the N terminus (mimicking a peptide bond). The structure calculations relied on 2051 meaningful upper distance limit values derived from the $^{1}$H,$^{1}$H NOE intensities and 156 dihedral angle constraints (Table 1). The average total target function for the family of 20 conformers with the lowest energy was 0.93 ± 0.06 Å$^2$ (CYANA calculations), and the root mean square deviation for residues 2–92 calculated with respect to the mean structure was 0.47 ± 0.08 Å for the backbone atoms and 0.86 ± 0.07 Å for the heavy atoms. After energy minimization with AMBER, the final cluster had a target function of 0.64 ± 0.09 Å$^2$, and the root mean square deviation increased to 0.56 ± 0.15 Å for the backbone and 0.96 ± 0.15 Å for the heavy atoms (Table 2).

**TABLE 1**
**Summary of the experimental constraints used in the structure determination of Tah1-MEEVD**

| Residues | All (116, Tah1 + MEEVD) | Structured (2–92, Tah1) |
|---|---|---|
| **NOE-based distance constraints** | | |
| Total | 2051 | 1896 |
| Intraresidue ($i = j$) | 359 | 321 |
| Sequential ($\|i - j\| = 1$) | 502 | 446 |
| Medium range ($1 < \|i - j\| < 5$) | 680 | 651 |
| Long range ($\|i - j\| \geq 5$) | 505 | 478 |
| Intermolecular | 5 | |
| NOEs/restrained residue | 18.5 | 20.8 |
| Hydrogen bond constraints | 8 | 8 |
| **Dihedral angle constraints** | | |
| $\varphi$ (degrees) | 78 | 78 |
| $\psi$ (degrees) | 78 | 78 |
| Total no. of constraints | 2215 | 2051 |
| Total no. of constraints/residue | 20.0 | 22.5 |
| Long range constraints/residue | 4.6 | 5.3 |

**TABLE 2**
**Summary of the quality statistics for the ensemble of 20 structures calculated for Tah1-MEEVD**

| Residues | All (116, Tah1 + MEEVD) | Structured (2–92, Tah1) |
|---|---|---|
| **Root mean square deviation values** | | |
| All backbone atoms | 3.8 Å | 0.56 Å |
| All heavy atoms | 4.1 Å | 0.96 Å |
| **Ramachandran plot from Procheck** | | |
| Most favored regions | 91.9% | 93.2% |
| Additionally allowed regions | 8.1% | 6.8% |
| Generously allowed regions | 0.0% | 0.0% |
| Disallowed regions | 0.0% | 0.0% |
| **Ramachandran plot from Richardson's laboratory** | | |
| Most favored regions | 97.6% | 98.2% |
| Allowed regions | 2.3% | 1.8% |
| Disallowed regions | 0.1% | 0.0% |
| **Structure quality factors: Overall statistics (mean score ± S.D.)** | | |
| Procheck G-factor ($\varphi/\psi$ only) | 0.22 | 0.26 |
| Procheck G-factor (all dihedral angles) | −0.09 | −0.07 |
| Verify3D | 0.19 ± 0.03 | 0.26 ± 0.04 |
| ProsaII (-ve) | 0.43 ± 0.05 | 0.64 ± 0.05 |
| MolProbity clashscore | 1.24 ± 0.96 | 1.14 ± 1.9 |
| **Structure quality factors: Overall statistics (*Z*-score)** | | |
| Procheck G-factor ($\varphi/\psi$ only) | 1.18 | 1.34 |
| Procheck G-factor (all dihedral angles) | −0.53 | −0.41 |
| Verify3D | −4.33 | −3.21 |
| ProsaII (-ve) | −0.91 | −0.04 |
| MolProbity clashscore | 1.31 | 1.33 |

The final family of 20 conformers of Tah1 obtained after energy minimization is shown in Fig. 1. The protein consists of five antiparallel α-helices (Fig. 1, *A* and *B*). Residues 2–33 (in *red*) form the first TPR motif, residues 38–66 (in *blue*) form the second TPR motif, and residues 73–91 (in *green*) form a long C helix that interacts mainly with helix 2B. The last 20 C-terminal residues of Tah1 (residues 92–111) are unstructured, with no long range NOEs involving protons in this segment of the protein (Table 1). The mobility of this unstructured region does not follow the general tumbling of the molecule. Some of the conformers of the family of structures present a $3_{10}$ helix encompassing residues 71–73 (shown in *orange* in the secondary structure schematic of Fig. 1*A*). The protein is stabilized by hydrophobic interactions mainly involving the following residues: Gly-11, Leu-14, Ala-23, Tyr-27, Leu-30, Ile-31, Ala-45, Leu-48, Ala-57, Cys-61, Gly-64, Leu-65, Leu-80, and Leu-84.

A positively charged channel ~11 Å wide and 21 Å long is formed by residues belonging to helices 1A, 2A, and C (Fig. 1, *C* and *D*). The MEEVD peptide resides in this channel and stabilizes Tah1. $^{1}H,^{15}N$ HSQC spectra of Tah1 in the presence and absence of MEEVD are very similar, indicating that the overall fold of the protein is not significantly affected by the presence of the peptide. The interaction between Tah1 and the pentapeptide is characterized by few low intensity NOEs (supplemental Fig. 1), which translates into a disordered ensemble of conformers for the peptide (Fig. 1*B*). However, the information obtained from these NOE values together with the docking calculations as well as the titration experiments described below provide a clear orientation of the peptide inside the Tah1 binding channel as shown in Fig. 1, *B–D*, with the peptide lying generally parallel to the helices forming the pocket.

*Tah1 Binding to MEEVD*—To identify Tah1 residues that interact with MEEVD, $^{1}H,^{15}N$ HSQC spectra were acquired for labeled Tah1 in the presence of increasing concentrations of MEEVD peptide (Tah1 at 0.6 mM and MEEVD titrated from 0 to 2.2 mM final concentration). According to these measurements and assuming a single binding site, the measured affinity of Tah1 for the peptide is on the order of 1 μM. By mapping the chemical shift changes observed in the titration to the Tah1 structure, residues of Tah1 affected by MEEVD binding can be identified (Fig. 2). Resonance changes with $\Delta\delta_{avg}^{HN} = (((\Delta\delta^{H})^2 + (\Delta\delta^{N}/5)^2)/5)^{1/2}$ (in ppm) values that are more than one S.D. away

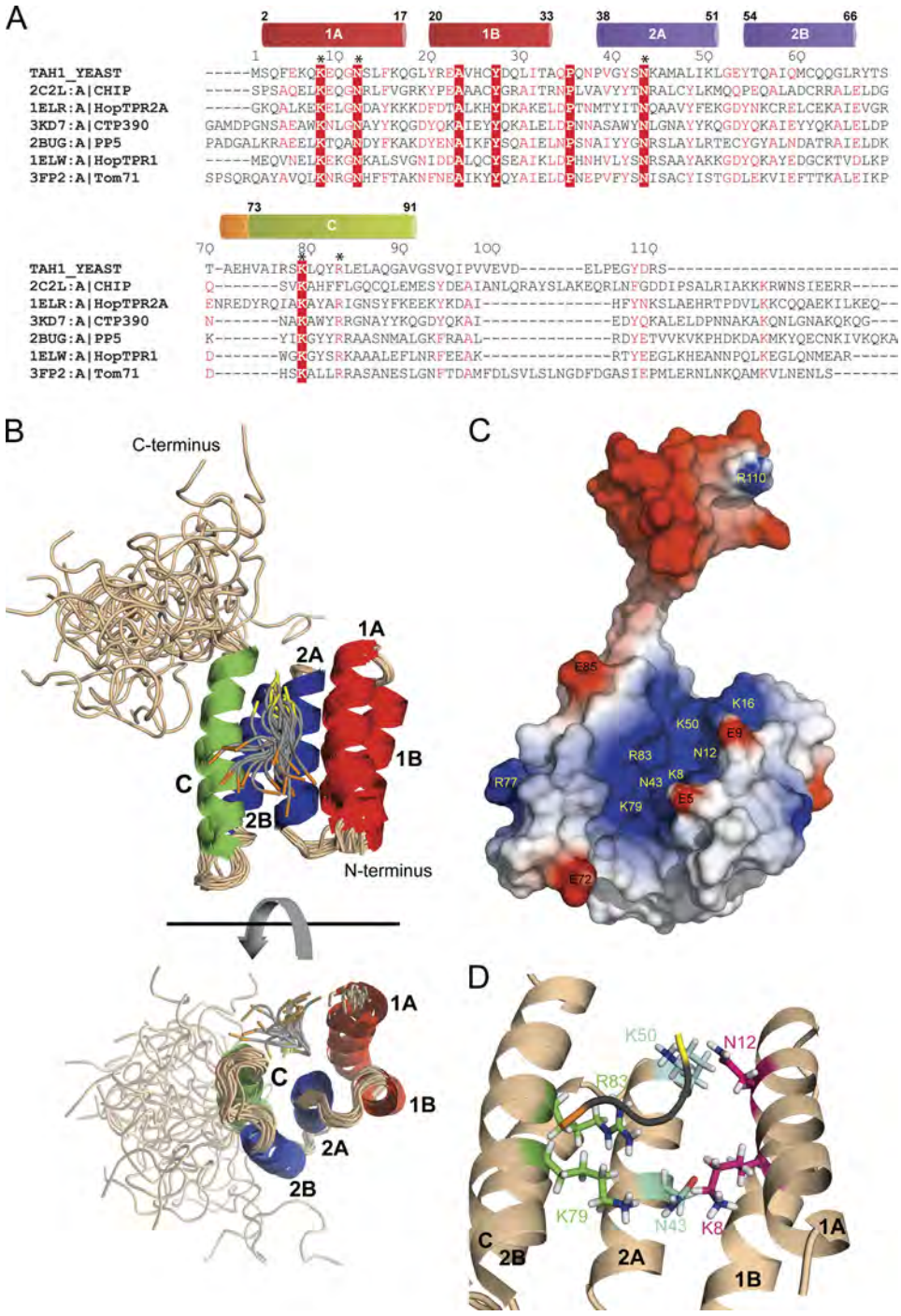


FIGURE 1. **Tah1 solution structure.** *A*, alignment of yeast Tah1 with TPR domains of mouse CHIP (22), human HOP (21), the engineered protein CTP390 (16), G83R human serine/threonine protein phosphatase 5 (23), and *S. cerevisiae* Tom71 (24). The structures of all of these domains have been solved with a bound EEVD peptide. The secondary structure sequence of Tah1 is highlighted on *top* with the helical boundaries indicated. The five highly conserved residues forming the dicarboxylate clamp are indicated by an *asterisk*. In the alignment, identical residues are shown in *white* and *highlighted* in *red*, whereas highly similar residues are shown in *red*. The alignment was done using ClustalW2 (43) with default parameters followed by manual inspection and drawn using ESPript (44). *B*, *ribbon representation* of the 20 lowest energy conformers of the NMR solution structure of Tah1 bound to MEEVD. The first TPR motif is *colored* in *red*, the second in *blue*, and the C helix in *green*. Helices are labeled according to the common TPR nomenclature. The last 20 amino acids of Tah1 are unstructured. The MEEVD peptide is in *gray* with its N terminus in *orange* and its C terminus in *yellow*. *C*, the electrostatic surface potential (*red*, $<-3$ *kT/e*; blue, $>3$ *kT/e*) of the lowest energy conformer of Tah1 calculated using DelPhi (45) is shown with the positively charged channel facing the reader. Some residues of interest are *highlighted*. *D*, a close-up view of the Tah1 channel of the lowest energy conformer. Side chains of the residues contributing to the positively charged channel are shown in *stick representation* with nitrogen in *blue*, oxygen in *red*, and hydrogen in *white*. Carbon is *colored pink* for Lys-8 and Asn-12 in helix 1A, *cyan* for Asn-43 and Lys-50 in helix 2A, and *bright green* for Lys-79 and Arg-83 in helix C. All structure figures were generated using PyMOL (Schrodinger LLC, New York).

from the mean value were selected as being significant. Many residues that exhibit significant changes in chemical shift are located in helix 2A (Gly-40, Asn-43, Lys-44, Ala-45, Ala-47, Leu-48, and Lys-50), which forms the base of the channel where the pentapeptide binds. In addition, there are some residues with high $\Delta\delta_{avg}^{HN}$ values belonging to helix 1A (Asn-12, Leu-14,

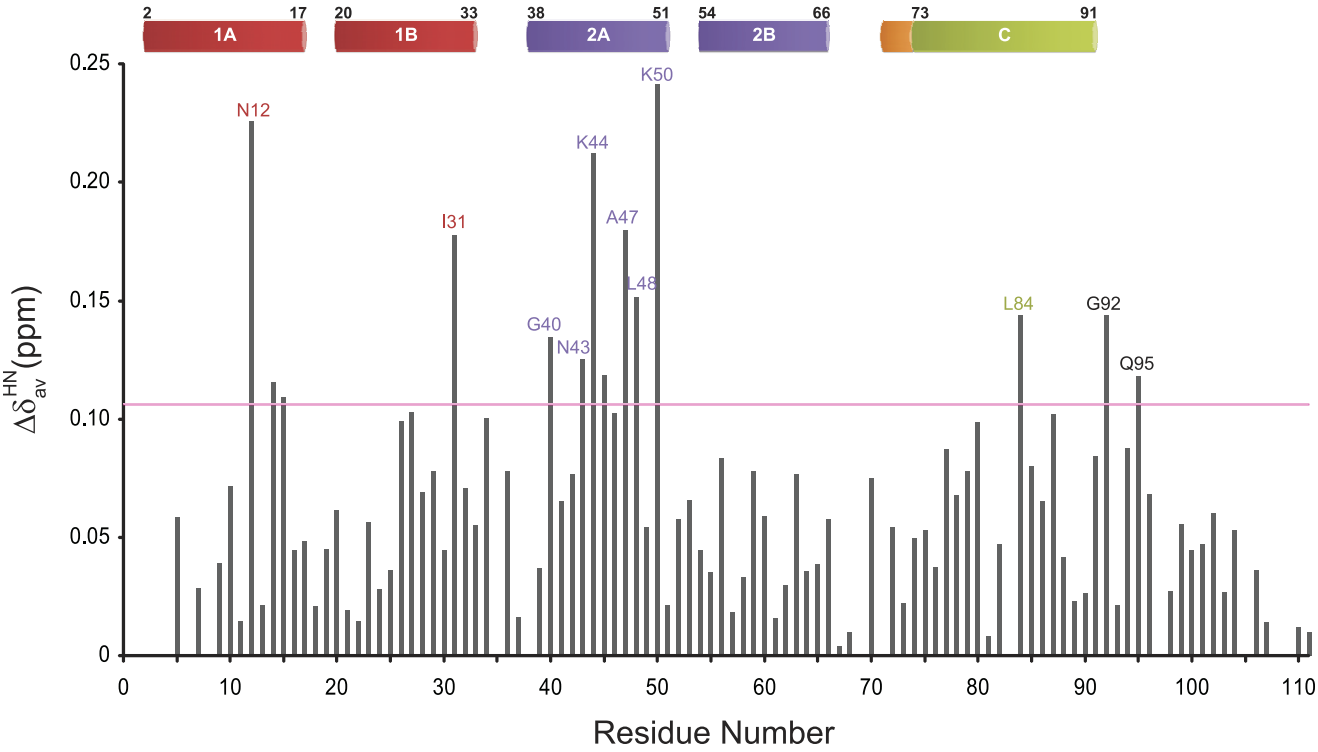


FIGURE 2. **Mapping the binding of MEEVD to Tah1 by NMR.** Shown is a plot of the weighted average chemical shift differences ($\Delta\delta^{HN}_{avg}$) in the $^{1}H,^{15}N$ HSQC spectrum between free Tah1 and Tah1 bound to MEEVD (1:10 protein/peptide). The *horizontal pink line* represents the value of $\Delta\delta^{HN}_{avg}$ that is one S.D. away from the mean value. The secondary structure of Tah1 is shown on *top*.

and Phe-15), helix 1B (Ile-31), helix C (Leu-84), and the unstructured region (Gly-92 and Gln-95). Residues Lys-6 and Lys-8 in helix 1A, Ser-69 and Ala-71 between helix 2B and helix C, and Arg-83 in helix C disappear due to line broadening. None of the residues in helix 2B showed a significant change in chemical shift, consistent with the fact that residues from helix 2B do not contribute to the channel (Fig. 1, *B–D*). Residues 1–4 do not appear in the HSQC spectra of the free or peptide-bound Tah1, and residues 108 and 109 in the unstructured region do not shift, whereas residues 35, 38, 97, and 105 are prolines.

Complementary experiments were carried out by titrating $^{15}N$-labeled Tah1 with unlabeled Hsp82-MC (residues 260–709 of yeast Hsp82; Tah1 at 200 $\mu$M and Hsp82-MC titrated from 0 to 400 $\mu$M). The addition of 2 eq of Hsp82-MC to Tah1 caused the complete disappearance of the $^{1}H,^{15}N$ HSQC signals due to relaxation apart from those belonging to the unstructured C-terminal region of Tah1. The addition of 0.5 eq of Hsp82-MC to Tah1 demonstrated that residues most affected by Hsp82-MC binding to Tah1 are located in the channel created by the three $\alpha$-helices, as observed with the peptide (data not shown).

In parallel with the NMR titration experiments, binding studies of Tah1 and Tah1 mutants to MEEVD were also carried out using ITC experiments (supplemental Fig. 2) to determine residues critical for mediating this interaction. The mutational studies were based on the NMR titration results of Fig. 2 as well as on the alignment shown in Fig. 1*A* of other TPR domains whose structures were solved in complex with an EEVD peptide. Based on these structures, it was found that five highly conserved residues are typically involved in mediating electrostatic interactions with the peptide and form a two-carboxylate clamp that tightly interacts with the ultimate Asp-0 residue of the bound peptide. These residues are also conserved in Tah1, namely Lys-8, Asn-12, Asn-43, Lys-79, and Arg-83 (Fig. 1, *A*, *C*, and *D*). Asn-12 and Asn-43 show significant chemical shift changes upon MEEVD binding to Tah1 (Fig. 2), whereas the $^{1}H,^{15}N$ HSQC signals of Lys-8 and Arg-83 disappear, indicating chemical exchange. No significant chemical shift changes were detected for Lys-79; however, Leu-84, which is directly after Arg-83, exhibits significant chemical shift changes (Fig. 2), indicating that the peptide binds to this region of the protein. The measured dissociation constant ($K_d$) by ITC for the Tah1-MEEVD interaction is 0.55 $\pm$ 0.06 $\mu$M, similar to that obtained by NMR above, with a stoichiometry of about 1:1 (Table 3). The interaction is mainly enthalpically driven. The positive entropy of binding might reflect the release of water molecules from the binding site upon the interaction of MEEVD with Tah1. Consistent with the known complex structures and with our NMR titration experiments, mutation of residues that form the two-carboxylate clamp either reduces (K8A and N12A of helix 1A) or abolishes (N43A of helix 2A, K79A and R83A of helix C) binding of MEEVD to Tah1. Furthermore, Mutation of the Lys-50 residue of helix 2A, which exhibited the highest chemical shift change upon MEEVD titration (Fig. 2), was found to reduce peptide binding affinity to Tah1. All of these residues form the positively charged channel of Tah1 (Fig. 1*D*).

Interestingly, Lys-79 and Arg-83 are part of helix C in Tah1 rather than of helix 3A of a third TPR motif as in the case of the other TPR domain proteins (Fig. 1*A*). Indeed, removal of helix C by truncating Tah1 at residue 74 (Tah1(1–74)) results in a

**TABLE 3**
**Thermodynamic parameters for the interaction of MEEVD peptide with Tah1 and its mutants**

| Protein | $K_d$ | $\Delta G$ | $\Delta H$ | $\Delta S$ | $n$ |
|---|---|---|---|---|---|
| | $\mu$M | kcal mol$^{-1}$ | kcal mol$^{-1}$ | cal mol$^{-1}$ K$^{-1}$ | |
| Tah1 | 0.55 (0.06)[a] | −7.9 (0.1) | −6.9 (0.1) | 3.8 (0.4) | 1.14 (0.01) |
| Tah1(K8A) | 36.76 (13.11) | −5.6 (2.0) | −5.3 (1.5) | 1.1 (5.4) | 1.26 (0.24) |
| Tah1(N12A) | 18.83 (3.26) | −6.0 (0.1) | −4.6 (0.7) | 4.9 (2.4) | 0.76 (0.08) |
| Tah1(N43A) | No binding | No binding | No binding | No binding | No binding |
| Tah1(K50A) | 23.20 (6.64) | −5.9 (0.2) | −4.9 (0.8) | 3.6 (3.0) | 1.17 (0.01) |
| Tah1(Q56A) | 0.65 (0.06) | −7.8 (0.1) | −7.0 (0.1) | 3.1 (0.3) | 1.17 (0.01) |
| Tah1(R66A) | 0.83 (0.10) | −7.7 (0.1) | −7.6 (0.1) | 0.3 (0.5) | 1.09 (0.01) |
| Tah1(K79A) | No binding | No binding | No binding | No binding | No binding |
| Tah1(R83A) | No binding | No binding | No binding | No binding | No binding |
| Tah1(1–74) | No binding | No binding | No binding | No binding | No binding |
| Tah1(1–93) | 0.30 (0.06) | −8.3 (0.1) | −3.2 (0.1) | 18.4 (0.4) | 0.73 (0.01) |

[a] Numbers in parenthesis represent S.D.

soluble protein that has only two TPR motifs but that cannot bind the MEEVD peptide (Table 3). On the other hand, removal of the unstructured region of Tah1 (Tah1(1–93)) does not significantly affect peptide binding and gives a similar $K_d$ and $n$ as WT protein but a higher $\Delta S$, possibly indicating higher solvent contribution upon peptide binding to Tah1. Finally, consistent with the NMR results of Fig. 2, mutation of residues in helix 2B (Q56A and R66A) has no effect on MEEVD binding to Tah1.

*C Termini of Tah1 and Pih1 Are Required for Tah1-Pih1 Interaction*—We had proposed and shown earlier that Tah1 forms a ternary complex with Hsp90 and Pih1 (2). This was based on pull-down assays, yeast two-hybrid screens, and functional assays. Pih1 itself was found to be an unstable protein that is stabilized by its interactions with Tah1 and Hsp90. We found that the C terminus of Tah1 (residues 76–111; Figs. 1*A* and 3*A*) is required for its interaction with Pih1 (2). To further characterize the interaction between Tah1 and Pih1 and to understand how the stability of Pih1 is modulated by the Hsp90/Tah1 system, we mapped the interaction surface between Tah1 and Pih1 by size exclusion chromatography.

As we demonstrated before (2), full-length Pih1 protein has a tendency to aggregate and to form multiple oligomeric states that spread across the Superdex 200 size exclusion column (Fig. 3*B*). As shown in the figure, purified Pih1 typically migrates as two peaks on the column; one peak is close to the void volume, above 669 kDa, whereas the other peak is around 50 kDa, close to the molecular mass of a Pih1 monomer (see also Fig. 3*C*). Upon isolation, this monomeric Pih1 did not readily reaggregate within the time frame of the experiment (Fig. 3, *B* and *C*, *a*). Because Pih1 does not contain any known motifs, we examined the Pih1 sequence and noticed that the Pih1 C-terminal region contains hydrophobic and proline-rich patches. Several C-terminal truncation constructs were then made to find a stable and well behaved fragment of this protein. Pih1(1–230) and Pih1(1–284) had such characteristics. Both, Pih1(1–230) and Pih1(1–284) eluted as monomers on Superdex 200 (Fig. 3*B*) and Superdex 75 size exclusion columns (Fig. 3*C*, *a*). These observations suggest that the aggregation-prone property of Pih1 might result mainly from the Pih1 C-terminal sequence (addressed further below).

In order to stabilize Pih1, we initially naively fused full-length Pih1 to full-length Tah1. The Pih1-Tah1 fusion construct spreads out and runs predominantly as large oligomers and higher order aggregates on a Superdex 200 column (Fig. 3*B*). However, when Pih1 is fused to the C-terminal 75–111 fragment of Tah1, which contains the C helix and the unstructured region of Tah1 (Fig. 1, *A* and *B*), the Pih1-Tah1(75–111) fusion protein migrates as a stable, possibly monomeric protein (Fig. 3*B*). This is consistent with our earlier observation that Pih1 physically interacts with Tah1 through the Tah1 C terminus (2). When Pih1 is fused to the unstructured C-terminal region of Tah1, the Pih1-Tah1(94–111) fusion protein migrates as higher order oligomers, similar to the Pih1-Tah1 fusion protein. These results suggest that amino acid residues in the C helix and the unstructured region of Tah1 may play an important role in stabilizing the interaction of Pih1 with Tah1. The aggregation of the Pih1-Tah1 fusion might be due to destabilizing steric structural clashes present in such a bigger fusion.

Consistent with the requirement for the C terminus of Tah1 to mediate the Tah1-Pih1 interaction, the deletion of the C helix and the unstructured region of Tah1 (Tah1(1–74)) or only of the unstructured region (Tah1(1–93)) abolished the binding to Pih1 (Fig. 3*C*, *b*). Note that, unexpectedly, Tah1(1–93) migrates faster than Tah1 or Tah1(1–74) on the size exclusion column for undetermined reasons. The deletion of the C terminus of Pih1 also abolished the binding of Tah1 to Pih1 (Fig. 3*C*, *c*). Hence, the C terminus of Pih1 is required for binding to Tah1. This was further confirmed by observing that the isolated Pih1(231–344) fragment can bind to Tah1 (Fig. 3*D*). This is in agreement with a recent report showing that residues 199–344 of Pih1 are sufficient for binding to Tah1 (36). Finally, the presence of excess MEEVD peptide did not abolish the Pih1-Tah1 interaction (Fig. 3*C*, *d*), suggesting the presence of a Pih1-Tah1-MEEVD ternary complex, which is consistent with our proposal of the presence of Pih1-Tah1-Hsp90 ternary complex (2).

*C Terminus of Pih1 Destabilizes the Protein*—The C terminus of Pih1 seems to play a major role in the destabilization and aggregation of the purified protein *in vitro* (Fig. 3*B*). To assess whether this is also true *in vivo*, initially, WT and *rpt6-25* mutant yeast cells (a proteasome *ts* mutant) expressing full-length EGFP-Pih1 (enhanced GFP fused to the N terminus of Pih1) were grown to midlog phase at room temperature, and then the temperature was shifted to 37 °C for 2 h (Fig. 4*A*). At the indicated time points, EGFP-Pih1 was visualized *in vivo* using confocal fluorescence microscopy. At the permissive temperature (room temperature), EGFP-Pih1 was distributed in the cytoplasm and nucleus in both WT and *rpt6-25* strains. However, although EGFP-Pih1 localization was unchanged in the WT strain at 37 °C, the inhibition of proteasome-mediated degradation in *rpt6-25* strain at this non-permissive temperature induced rapid recruitment of EGFP-Pih1 to discrete foci in

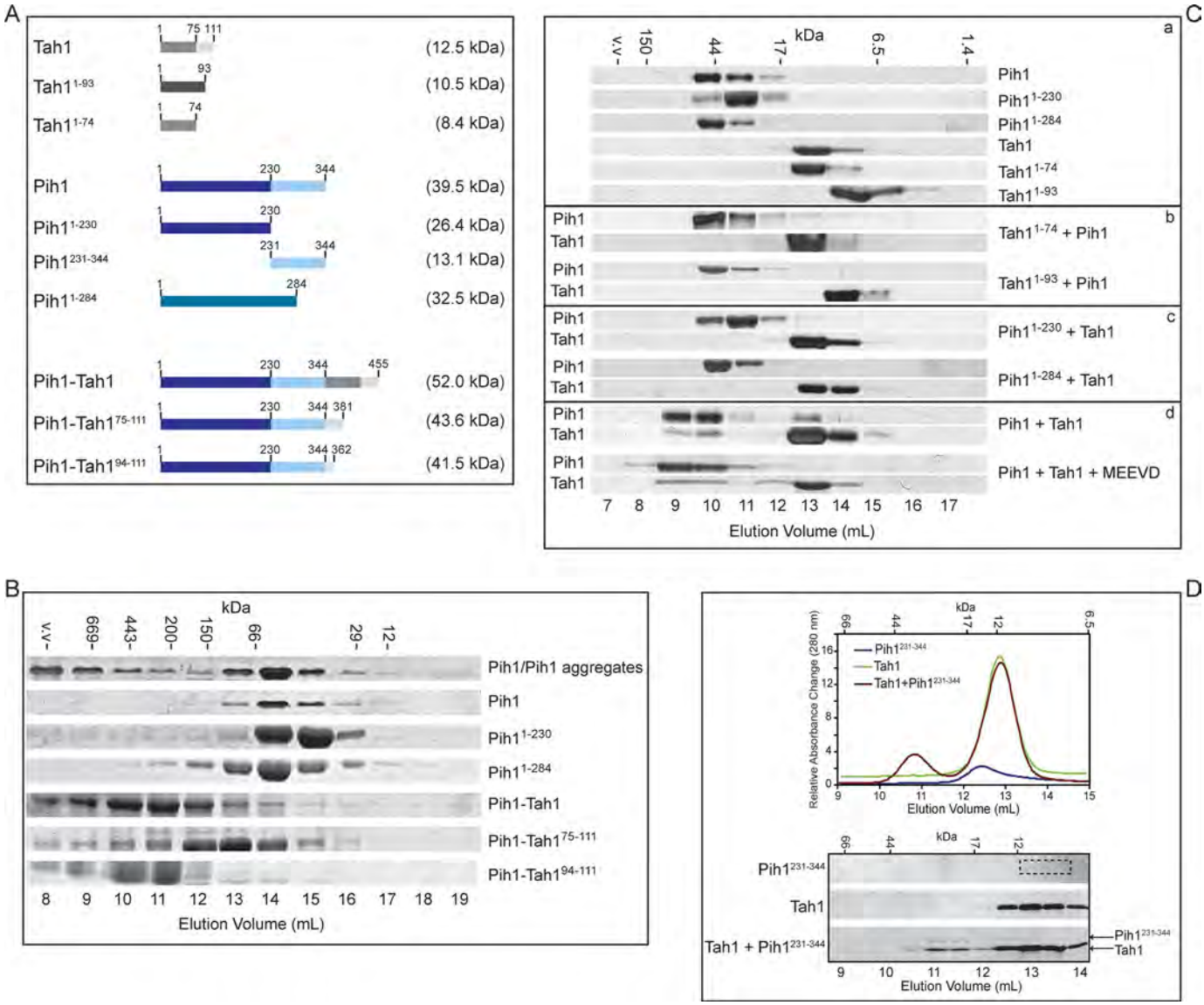


FIGURE 3. **Mapping the interaction between Tah1 and Pih1.** *A*, schematic diagram of the different Tah1 and Pih1 constructs used in the binding experiments. The theoretical molecular weights of the constructs are provided on the *right*. *B*, size exclusion chromatography of Pih1 constructs on Superdex 200 column. The elution volume is indicated at the *bottom*, and the elution positions of the molecular weight standards are indicated at the *top* of the *lanes*. *C*, elution profiles for the different Pih1 (*panel a*), Tah1 (*panel a*), and Pih1 + Tah1 (*panels b–d*) constructs on a Superdex 75 column. *D*, elution profiles of Tah1 (100 $\mu$g), Pih1(231–344) (100 $\mu$g), and the mixture of Tah1 (100 $\mu$g) and Pih1(231–344) (100 $\mu$g) on a Superdex 75 column as observed by absorbance at 280 nm (*top*) or SDS-PAGE analysis (*bottom*).

the cytoplasm. These cytoplasmic foci became more prominent after 2 h of incubation at 37 °C. The clustering of EGFP-Pih1 in the cytoplasm was fully reversible because shifting the temperature back to room temperature led to the complete dissipation of the foci within 45 min. We hypothesized that these cytoplasmic foci of Pih1 may resemble those formed by misfolded proteins like von Hippel-Lindau (VHL) factor when expressed in yeast. The proper folding of VHL requires the presence of its cofactor elongin BC (37); the absence of elongin BC leads to the misfolding, ubiquitination, and subsequent degradation of VHL in WT yeast cells (38). Therefore, EGFP-Pih1 was co-expressed with ChFP-VHL (cherry fluorescent protein fused to the N terminus of VHL) in *rpt6-25* strain to assess whether aggregated Pih1 was with the VHL misfolded protein foci. Complete colocalization of EGFP-Pih1 with ChFP-VHL (Fig. 4*B*) was observed, suggesting that cytoplasmic foci of EGFP-Pih1 consist of misfolded EGFP-Pih1.

To explicitly test whether the C terminus of Pih1 is responsible for destabilizing the protein, GFP was fused to the 282–344 C-terminal fragment of Pih1, and the localization of this fusion protein, GFP-Pih1(282–344), was assessed in both WT and *rpt6-25* mutant cells. We observed GFP-Pih1(282–344) aggregation in 70% of mutant cells but not in WT cells, even at the permissive temperature (Fig. 4*C*). Furthermore, GFP-Pih1(282–344) was rapidly degraded when translation was arrested by the addition of cyclohexamide in log phase WT cells, whereas GFP was stable (Fig. 4*D*). This is also consistent with our previous observation that the depletion of endogenous Tah1 in yeast results in the rapid degradation of endogenous Pih1 (2).

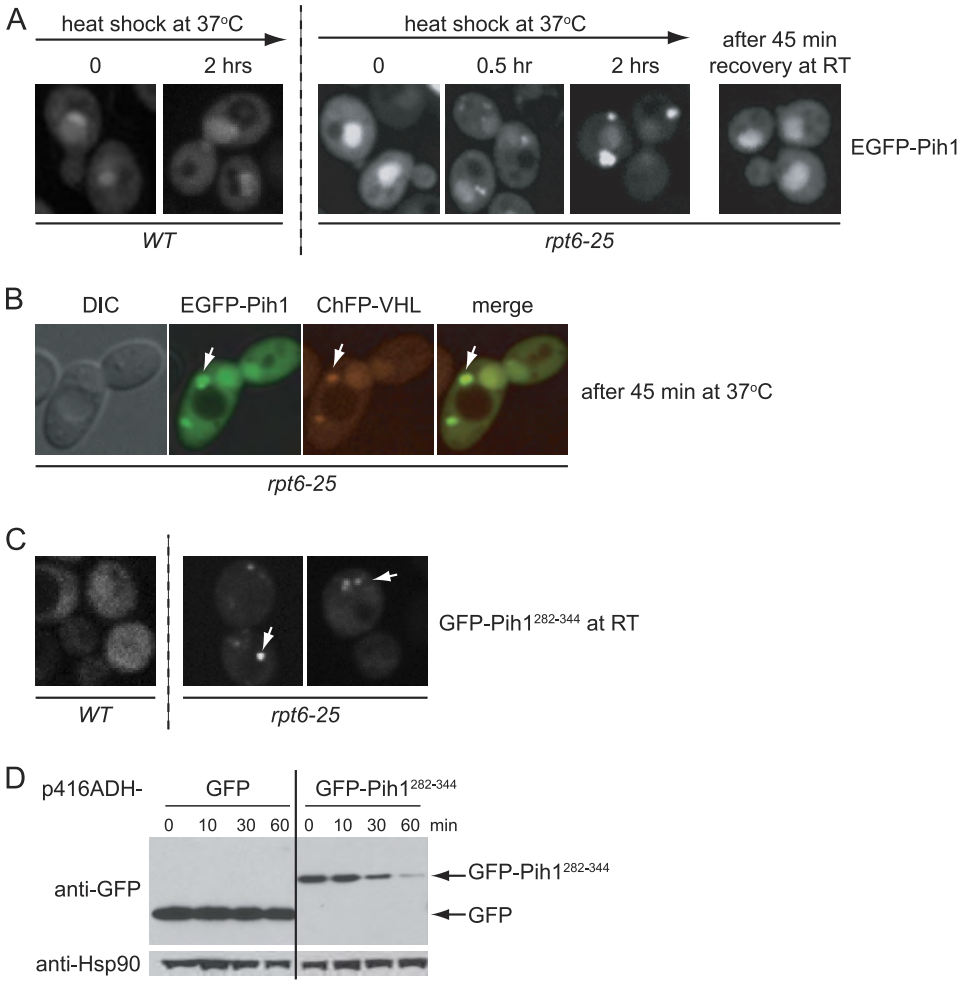


FIGURE 4. **The C terminus of Pih1 destabilizes the protein.** *A*, shown are confocal fluorescence images of S288C WT and *rpt6-25* yeast cells expressing EGFP-Pih1. The cells were grown at room temperature (*RT*) and then exposed to heat shock for 2 h. The *rpt6-25* cells were then allowed to recover at room temperature. *B*, confocal fluorescence images of *rpt6-25* cells co-expressing EGFP-Pih1 (*green*) and ChFP-VHL (*red*) after exposure to heat shock for 45 min. *C*, confocal fluorescence images of S288C WT and *rpt6-25* cells expressing GFP-Pih1(282–344) at room temperature. *D*, Western blot, using anti-GFP antibodies, of W303 WT cells expressing GFP or GFP-Pih1(282–344) grown to midlog phase after treatment with cyclohexamide to arrest translation. The Western blot against Hsp90 is shown as a control.

These results strongly suggest that the C terminus of Pih1 is responsible for Pih1 instability and aggregation. Furthermore, it is interesting to note that Pih1(282–344) can act as a degradation tag in yeast.

## DISCUSSION

The structure of Tah1 is rather unique in that it has only two TPR motifs and a C helix and yet is stable and able to bind the MEEVD peptide. All other known TPR domains that interact with Hsp90/Hsp70 consist of three TPR motifs and a capping helix (Fig. 1*A*). Hence, the structure of Tah1 was rather unexpected (39). The C helix of Tah1 is not a regular solubility helix as it appears in other TPR proteins, because it hosts two of the five highly conserved residues that establish electrostatic interactions with MEEVD (Figs. 1 and 2 and Table 3). Hence, the C helix serves the role of the third TPR motif in other domains. The dissociation constant of 0.5 $\mu$M that we obtained for MEEVD binding to Tah1 by ITC and NMR measurements is consistent with the one obtained for the hepta- and decapeptides described by Millson *et al.* (39); however, it differs from that for the unprotected peptide, which was reported to have a $K_d$ of about 35 $\mu$M. It is also consistent with the $K_d$ obtained for full-length Hsp90 binding obtained by Eckert *et al.* (36).

The major overall difference between the structure of Tah1 and that of other TPR domains that bind Hsp90/Hsp70 is that helix 1A and helix C are closer to helix 2A than they are in the other TPR repeat proteins, and, as a result, the binding channel is narrower (Fig. 5). Also, helix 2B appears to be slightly further away from helix 2A in Tah1 compared with other TPR domains. It is reasonable to suggest that this tight packing of helices contributes to the stability of Tah1. The majority of residues that are typically conserved in TPR domains and that are critical for stabilizing the hydrophobic core of these proteins are conserved in Tah1 (40). Hence, Tah1 can be considered to be a minimal TPR domain protein that can bind to Hsp90/Hsp70. The only other minimal stable TPR domain that we know of is that of rat Tom20 (95 residues), which has only one TPR that binds to the mitochondrial targeting presequence but not to Hsp90/Hsp70 (41).

Helices 1B and 2A of Tah1 are closest in terms of primary sequence and length to the consensus helices found in TPR

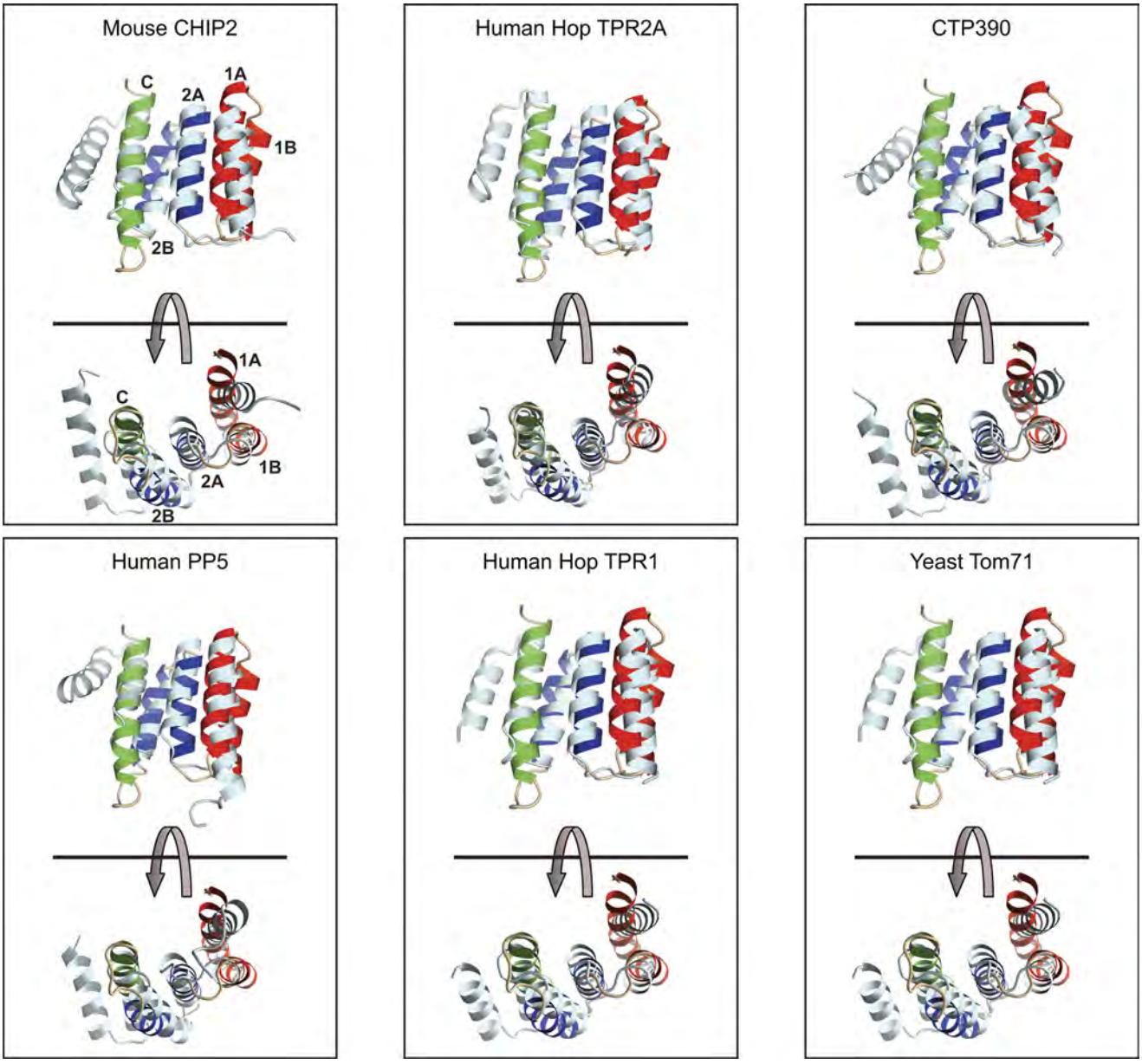


FIGURE 5. **Comparison of Tah1 structure with that of other TPR domains.** Shown is the *ribbon representation* of the lowest energy Tah1 structure without the unstructured region overlaid with the three TPR motifs (in *white*) of mouse CHIP2 (Protein Data Bank entry 2C2L) (22), human Hop TPR2A (1ELR) (21), the engineered protein CTP390 (3KD7) (16), human G83R protein phosphatase 5 TPR domain (2BUG) (23), human Hop TPR1 (1ELW) (21), and *S. cerevisiae* Tom71 (3FP2) (24). The structure alignment was carried out in Coot (available on the York Structural Biology Web site) (46).

motifs, which are typically 14 residues long (40). Helix 1A of Tah1 consists of 16 residues and has an additional turn at the C terminus (Fig. 5). In contrast, helix 1A in Tom71 and protein phosphatase 5 is 20 and 19 residues long, respectively, with the additional turns present at the N terminus of the helix. Helix 2B of Tah1 (12 residues) is shorter than that of equivalent helices in the other domains of the family, but helix C (18 residues), which is the equivalent of helix 3A in other domains, is longer. The angle between the two helices within a TPR motif in Tah1 is similar to that measured for other TPR motifs and is about 155–165°.

The NMR measurements of Fig. 2 and the binding experiments of Fig. 3, coupled with the single point mutation ITC results (Table 1 and supplemental Fig. 2), indicate that the amino acid residues involved in binding the Hsp90 C-terminal sequence are Lys-8, Asn-12, Asn-43, Lys-50, Lys-79, and Arg-83. These results are in agreement with our previous (2) and current data showing that neither TPR motifs of Tah1 alone (Tah1(1–75)) nor the C terminus of Tah1(76–111) can bind to Hsp90 on its own. Instead, the five helices of Tah1 are necessary for the binding.

The binding of Tah1 to Pih1 stabilizes Pih1 and is found to be mediated by the C-terminal unstructured regions in the respective proteins. The C helix and the unstructured region of Tah1 are required for this interaction (Fig. 3, *B* and *C*). Although we currently have no structural information on the fold of the Pih1 C terminus, it is predicted, using Jpred (42), to predominantly consist of $\beta$ strands. However, this region of the protein seems to be "problematic" because it leads to Pih1 aggregation *in vitro* (Fig. 3*B*) or to its destabilization *in vivo* (Fig. 4). Furthermore, Pih1(282–344) can lead to the degradation of GFP *in vivo* (Fig. 4*D*). It is interesting to note

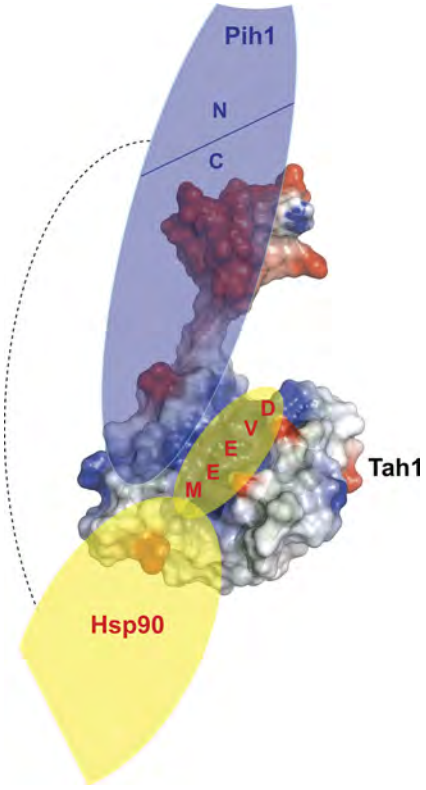


FIGURE 6. **Model of the Hsp90-Tah1-Pih1 complex.** Model of the complex formed by Pih1 (*blue*), Tah1 (represented by its electrostatic surface potential), and Hsp90 (*yellow*) based on the results of our analysis. The C-terminal region of Pih1 interacts with the C helix and the unstructured C terminus of Tah1, whereas the MEEVD peptide at the very C terminus of Hsp90 binds in the positively charged channel of Tah1. Data also indicate that Pih1 and Hsp90 directly interact (*dotted line*).

that the pI of Pih1(231–344) and Pih1(282–344) is 9.3 and 9.7, respectively, whereas the pI of Tah1(75–111) and Tah1(94–111) is 4.7 and 3.8 (also see Fig. 1*C*), respectively. Hence, the stabilizing interaction between these two proteins is expected to be mainly electrostatic.

In Fig. 6, we present a schematic of the interactions of Tah1 with Hsp90 and Pih1. Our experiments suggest that the Hsp90 C terminus will bind within the channel formed by Tah1. On the other hand, the C terminus of Tah1 will form strong interactions with the C terminus of Pih1. However, our earlier data (2) as well as those of others (36) suggest that Hsp90 directly binds Pih1 as well. Such a positioning of binding partners would allow this small TPR domain protein to form a ternary complex with Hsp90 and Pih1. Our data collectively suggest that Tah1 is essential for the formation of the Hsp90-Tah1-Pih1 ternary complex that stabilizes Pih1.

*Acknowledgments—We thank Dr. Francesca Cantini and Prof. Antonio Rosato for help with the structure calculations and software usage. We thank Dr. Hermann Torsten for help with UNIO. We thank Elisa Leung and Usheer Kanjee for help with the ITC experiments and Dr. Majida El Bakkouri for help with the structure figures. A.P.-L. and B. J. acknowledge the WeNMR project (European FP7 e-Infrastructure grant, Contract 261572) for use of Web portals, computing, and storage facilities and CERM (University of Florence) for technical support.*

## REFERENCES

1. Zhao, R., Davey, M., Hsu, Y. C., Kaplanek, P., Tong, A., Parsons, A. B., Krogan, N., Cagney, G., Mai, D., Greenblatt, J., Boone, C., Emili, A., and Houry, W. A. (2005) Navigating the chaperone network. An integrative map of physical and genetic interactions mediated by the hsp90 chaperone. *Cell* **120,** 715–727
2. Zhao, R., Kakihara, Y., Gribun, A., Huen, J., Yang, G., Khanna, M., Costanzo, M., Brost, R. L., Boone, C., Hughes, T. R., Yip, C. M., and Houry, W. A. (2008) Molecular chaperone Hsp90 stabilizes Pih1/Nop17 to maintain R2TP complex activity that regulates snoRNA accumulation. *J. Cell Biol.* **180,** 563–578
3. Jha, S., and Dutta, A. (2009) RVB1/RVB2. Running rings around molecular biology. *Mol. Cell* **34,** 521–533
4. Huen, J., Kakihara, Y., Ugwu, F., Cheung, K. L., Ortega, J., and Houry, W. A. (2010) Rvb1-Rvb2. Essential ATP-dependent helicases for critical complexes. *Biochem. Cell Biol.* **88,** 29–40
5. Boulon, S., Marmier-Gourrier, N., Pradet-Balade, B., Wurth, L., Verheggen, C., Jády, B. E., Rothé, B., Pescia, C., Robert, M. C., Kiss, T., Bardoni, B., Krol, A., Branlant, C., Allmang, C., Bertrand, E., and Charpentier, B. (2008) The Hsp90 chaperone controls the biogenesis of L7Ae RNPs through conserved machinery. *J. Cell Biol.* **180,** 579–595
6. Jeronimo, C., Forget, D., Bouchard, A., Li, Q., Chua, G., Poitras, C., Thérien, C., Bergeron, D., Bourassa, S., Greenblatt, J., Chabot, B., Poirier, G. G., Hughes, T. R., Blanchette, M., Price, D. H., and Coulombe, B. (2007) Systematic analysis of the protein interaction network for the human transcription machinery reveals the identity of the 7SK capping enzyme. *Mol. Cell* **27,** 262–274
7. Boulon, S., Pradet-Balade, B., Verheggen, C., Molle, D., Boireau, S., Georgieva, M., Azzag, K., Robert, M. C., Ahmad, Y., Neel, H., Lamond, A. I., and Bertrand, E. (2010) HSP90 and its R2TP/Prefoldin-like cochaperone are involved in the cytoplasmic assembly of RNA polymerase II. *Mol. Cell* **39,** 912–924
8. Horejsí, Z., Takai, H., Adelman, C. A., Collis, S. J., Flynn, H., Maslen, S., Skehel, J. M., de Lange, T., and Boulton, S. J. (2010) CK2 phospho-dependent binding of R2TP complex to TEL2 is essential for mTOR and SMG1 stability. *Mol. Cell* **39,** 839–850
9. Ni, L., Saeki, M., Xu, L., Nakahara, H., Saijo, M., Tanaka, K., and Kamisaki, Y. (2009) RPAP3 interacts with Reptin to regulate UV-induced phosphorylation of H2AX and DNA damage. *J. Cell. Biochem.* **106,** 920–928
10. Inoue, M., Saeki, M., Egusa, H., Niwa, H., and Kamisaki, Y. (2010) PIH1D1, a subunit of R2TP complex, inhibits doxorubicin-induced apoptosis. *Biochem. Biophys. Res. Commun.* **403,** 340–344
11. Hirano, T., Kinoshita, N., Morikawa, K., and Yanagida, M. (1990) Snap helix with knob and hole. Essential repeats in *S. pombe* nuclear protein nuc2+. *Cell* **60,** 319–328
12. Sikorski, R. S., Boguski, M. S., Goebl, M., and Hieter, P. (1990) A repeating amino acid motif in CDC23 defines a family of proteins and a new relationship among genes required for mitosis and RNA synthesis. *Cell* **60,** 307–317
13. D'Andrea, L. D., and Regan, L. (2003) TPR proteins. The versatile helix. *Trends Biochem. Sci.* **28,** 655–662
14. Yang, J., Roe, S. M., Cliff, M. J., Williams, M. A., Ladbury, J. E., Cohen, P. T., and Barford, D. (2005) Molecular basis for TPR domain-mediated regulation of protein phosphatase 5. *EMBO J.* **24,** 1–10
15. Smith, D. F. (2004) Tetratricopeptide repeat cochaperones in steroid receptor complexes. *Cell Stress Chaperones* **9,** 109–121
16. Cortajarena, A. L., Wang, J., and Regan, L. (2010) Crystal structure of a designed tetratricopeptide repeat module in complex with its peptide ligand. *FEBS J.* **277,** 1058–1066
17. Goebl, M., and Yanagida, M. (1991) The TPR snap helix. A novel protein repeat motif from mitosis to transcription. *Trends Biochem. Sci.* **16,** 173–177
18. Blatch, G. L., and Lässle, M. (1999) The tetratricopeptide repeat. A structural motif mediating protein-protein interactions. *BioEssays* **21,** 932–939
19. Wegele, H., Müller, L., and Buchner, J. (2004) Hsp70 and Hsp90. A relay team for protein folding. *Rev. Physiol. Biochem. Pharmacol.* **151,** 1–44
20. Pearl, L. H., and Prodromou, C. (2006) Structure and mechanism of the

Hsp90 molecular chaperone machinery. *Annu. Rev. Biochem.* **75,** 271–294
21. Scheufler, C., Brinker, A., Bourenkov, G., Pegoraro, S., Moroder, L., Bartunik, H., Hartl, F. U., and Moarefi, I. (2000) Structure of TPR domain-peptide complexes. Critical elements in the assembly of the Hsp70-Hsp90 multichaperone machine. *Cell* **101,** 199–210
22. Zhang, M., Windheim, M., Roe, S. M., Peggie, M., Cohen, P., Prodromou, C., and Pearl, L. H. (2005) Chaperoned ubiquitylation: Crystal structures of the CHIP U box E3 ubiquitin ligase and a CHIP-Ubc13-Uev1a complex. *Mol. Cell* **20,** 525–538
23. Cliff, M. J., Harris, R., Barford, D., Ladbury, J. E., and Williams, M. A. (2006) Conformational diversity in the TPR domain-mediated interaction of protein phosphatase 5 with Hsp90. *Structure* **14,** 415–426
24. Li, J., Qian, X., Hu, J., and Sha, B. (2009) Molecular chaperone Hsp70/Hsp90 prepares the mitochondrial outer membrane translocon receptor Tom71 for preprotein loading. *J. Biol. Chem.* **284,** 23852–23859
25. Savchenko, A., Yee, A., Khachatryan, A., Skarina, T., Evdokimova, E., Pavlova, M., Semesi, A., Northey, J., Beasley, S., Lan, N., Das, R., Gerstein, M., Arrowmith, C. H., and Edwards, A. M. (2003) Strategies for structural proteomics of prokaryotes. Quantifying the advantages of studying orthologous proteins and of using both NMR and X-ray crystallography approaches. *Proteins* **50,** 392–399
26. Bradford, M. M. (1976) A rapid and sensitive method for the quantitation of microgram quantities of protein utilizing the principle of protein-dye binding. *Anal. Biochem.* **72,** 248–254
27. Herrmann, T., Güntert, P., and Wüthrich, K. (2002) Protein NMR structure determination with automated NOE assignment using the new software CANDID and the torsion angle dynamics algorithm DYANA. *J. Mol. Biol.* **319,** 209–227
28. Cornilescu, G., Delaglio, F., and Bax, A. (1999) Protein backbone angle restraints from searching a database for chemical shift and sequence homology. *J. Biomol. NMR* **13,** 289–302
29. Dominguez, C., Boelens, R., and Bonvin, A. M. (2003) HADDOCK. A protein-protein docking approach based on biochemical or biophysical information. *J. Am. Chem. Soc.* **125,** 1731–1737
30. Bertini, I., Case, D. A., Ferella, L., Giachetti, A., and Rosato, A. (2011) Grid-enabled web portal for NMR structure refinement with AMBER. *Bioinformatics* **27,** 2384–2390
31. Bhattacharya, A., Tejero, R., and Montelione, G. T. (2007) Evaluating protein structures determined by structural genomics consortia. *Proteins* **66,** 778–795
32. Hu, Y., Rolfs, A., Bhullar, B., Murthy, T. V., Zhu, C., Berger, M. F., Camargo, A. A., Kelley, F., McCarron, S., Jepson, D., Richardson, A., Raphael, J., Moreira, D., Taycher, E., Zuo, D., Mohr, S., Kane, M. F., Williamson, J., Simpson, A., Bulyk, M. L., Harlow, E., Marsischky, G., Kolodner, R. D., and LaBaer, J. (2007) Approaching a complete repository of sequence-verified protein-encoding clones for *Saccharomyces cerevisiae*. *Genome Res.* **17,** 536–543
33. Alberti, S., Gitler, A. D., and Lindquist, S. (2007) A suite of Gateway cloning vectors for high-throughput genetic analysis in *Saccharomyces cerevisiae*. *Yeast* **24,** 913–919
34. Mumberg, D., Müller, R., and Funk, M. (1995) Yeast vectors for the controlled expression of heterologous proteins in different genetic backgrounds. *Gene* **156,** 119–122
35. Cliff, M. J., Williams, M. A., Brooke-Smith, J., Barford, D., and Ladbury, J. E. (2005) Molecular recognition via coupled folding and binding in a TPR domain. *J. Mol. Biol.* **346,** 717–732
36. Eckert, K., Saliou, J. M., Monlezun, L., Vigouroux, A., Atmane, N., Caillat, C., Quevillon-Chéruel, S., Madiona, K., Nicaise, M., Lazereg, S., Van Dorsselaer, A., Sanglier-Cianférani, S., Meyer, P., and Moréra, S. (2010) The Pih1-Tah1 cochaperone complex inhibits Hsp90 molecular chaperone ATPase activity. *J. Biol. Chem.* **285,** 31304–31312
37. Feldman, D. E., Thulasiraman, V., Ferreyra, R. G., and Frydman, J. (1999) Formation of the VHL-elongin BC tumor suppressor complex is mediated by the chaperonin TRiC. *Mol. Cell* **4,** 1051–1061
38. Kaganovich, D., Kopito, R., and Frydman, J. (2008) Misfolded proteins partition between two distinct quality control compartments. *Nature* **454,** 1088–1095
39. Millson, S. H., Vaughan, C. K., Zhai, C., Ali, M. M., Panaretou, B., Piper, P. W., Pearl, L. H., and Prodromou, C. (2008) Chaperone ligand-discrimination by the TPR-domain protein Tah1. *Biochem. J.* **413,** 261–268
40. Magliery, T. J., and Regan, L. (2004) Beyond consensus. Statistical free energies reveal hidden interactions in the design of a TPR motif. *J. Mol. Biol.* **343,** 731–745
41. Abe, Y., Shodai, T., Muto, T., Mihara, K., Torii, H., Nishikawa, S., Endo, T., and Kohda, D. (2000) Structural basis of presequence recognition by the mitochondrial protein import receptor Tom20. *Cell* **100,** 551–560
42. Cole, C., Barber, J. D., and Barton, G. J. (2008) The Jpred 3 secondary structure prediction server. *Nucleic Acids Res.* **36,** W197–201
43. Larkin, M. A., Blackshields, G., Brown, N. P., Chenna, R., McGettigan, P. A., McWilliam, H., Valentin, F., Wallace, I. M., Wilm, A., Lopez, R., Thompson, J. D., Gibson, T. J., and Higgins, D. G. (2007) ClustalW and ClustalX version 2.0. *Bioinformatics* **23,** 2947–2948
44. Gouet, P., Courcelle, E., Stuart, D. I., and Métoz, F. (1999) ESPript. Analysis of multiple sequence alignments in PostScript. *Bioinformatics* **15,** 305–308
45. Rocchia, W., Sridharan, S., Nicholls, A., Alexov, E., Chiabrera, A., and Honig, B. (2002) Rapid grid-based construction of the molecular surface and the use of induced surface charge to calculate reaction field energies. Applications to the molecular systems and geometric objects. *J. Comput. Chem.* **23,** 128–137
46. Emsley, P., Lohkamp, B., Scott, W. G., and Cowtan, K. (2010) Features and development of Coot. *Acta Crystallogr. D Biol. Crystallogr.* **66,** 486–501

## LEGEND FOR SUPPLEMENTARY FIGURE

**Supplementary Fig. 1. $^{15}$N-edited 2D $^{1}$H,$^{1}$H-NOESY spectrum**

2D NOESY spectrum highlighting a number of unambiguously assigned NOEs derived from the peptide. Black labels correspond to intra-peptide NOEs, while red labels correspond to inter-molecular NOEs. Intra-peptide NOEs were consistently more intense than inter-molecular NOEs suggesting a labile interaction between the peptide and the protein. These NOEs were essential to establish the orientation of the peptide in the protein channel, but they did not affect the Tah1 overall structure.

**Supplementary Fig. 2. ITC binding curves for the interaction of the MEEVD peptide with Tah1 and its mutants**

The upper panels show the calorimetric titrations for 26 injections of 450 μM of MEEVD peptide into 30 μM of Tah1 or its mutants with 150 s between injections. The lower panels show the integrated heat values from the upper panels as a function of the peptide/Tah1 molar ratio in the cell. The solid lines trace the best fit to the experimental points using the n identical independent binding sites model. The binding parameters are given in Table 3.

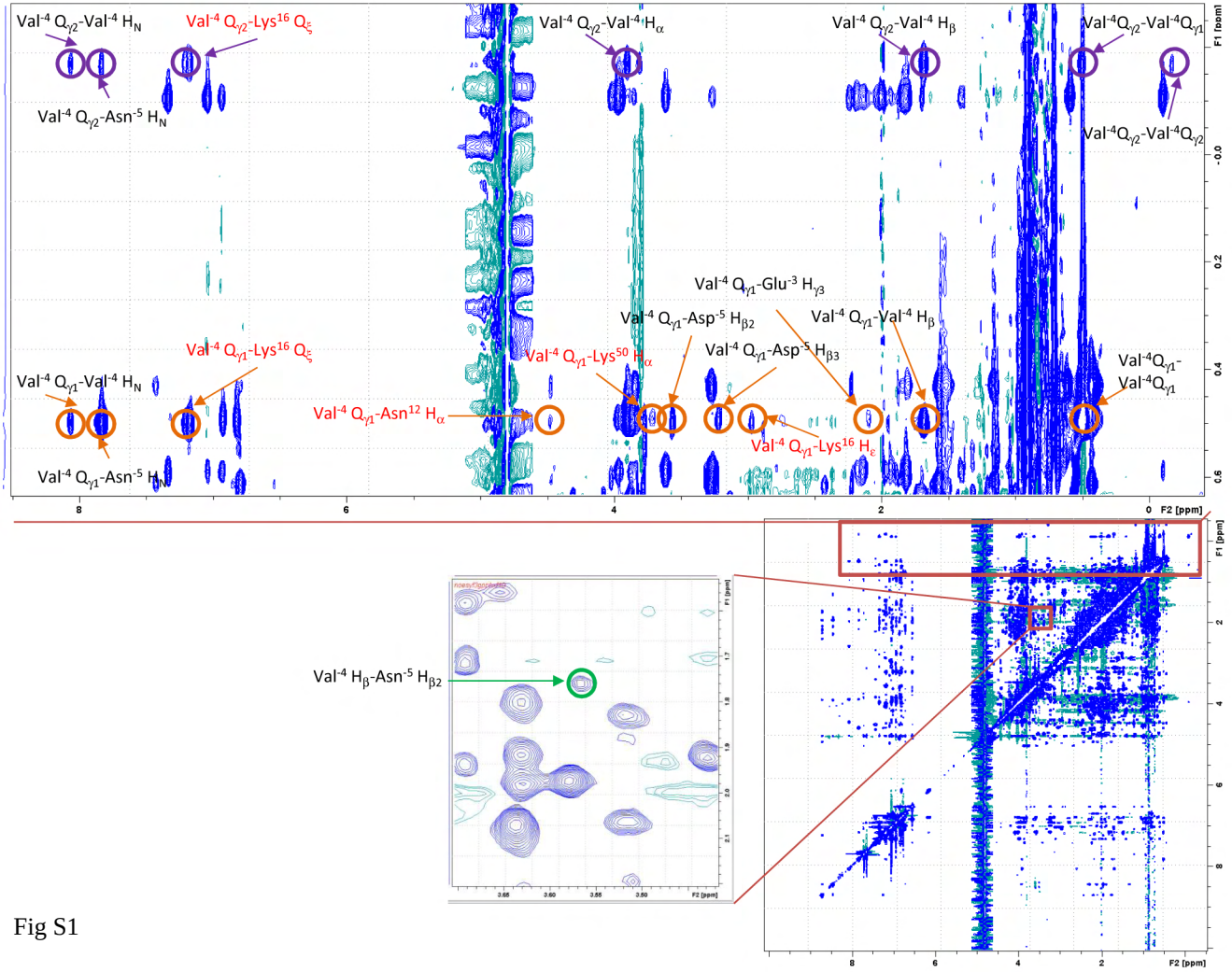
Val-4 Qγ2-Val-4 HN
Val-4 Qγ2-Lys16 Qξ
Val-4 Qγ2-Asn-5 HN
Val-4 Qγ2-Val-4 Hα
Val-4 Qγ2-Val-4 Hβ
Val-4 Qγ2-Val-4 Qγ1
Val-4 Qγ2-Val-4 Qγ2
Val-4 Qγ1-Glu-3 Hγ3
Val-4 Qγ1-Asp-5 Hβ2
Val-4 Qγ1-Val-4 Hβ
Val-4 Qγ1-Lys16 Qξ
Val-4 Qγ1-Val-4 HN
Val-4 Qγ1-Lys50 Hα
Val-4 Qγ1-Asp-5 Hβ3
Val-4 Qγ1-Val-4 Qγ1
Val-4 Qγ1-Asn12 Hα
Val-4 Qγ1-Lys16 Hε
Val-4 Qγ1-Asn-5 HN
F1 [ppm]
F2 [ppm]
Val-4 Hβ-Asn-5 Hβ2

Fig S1

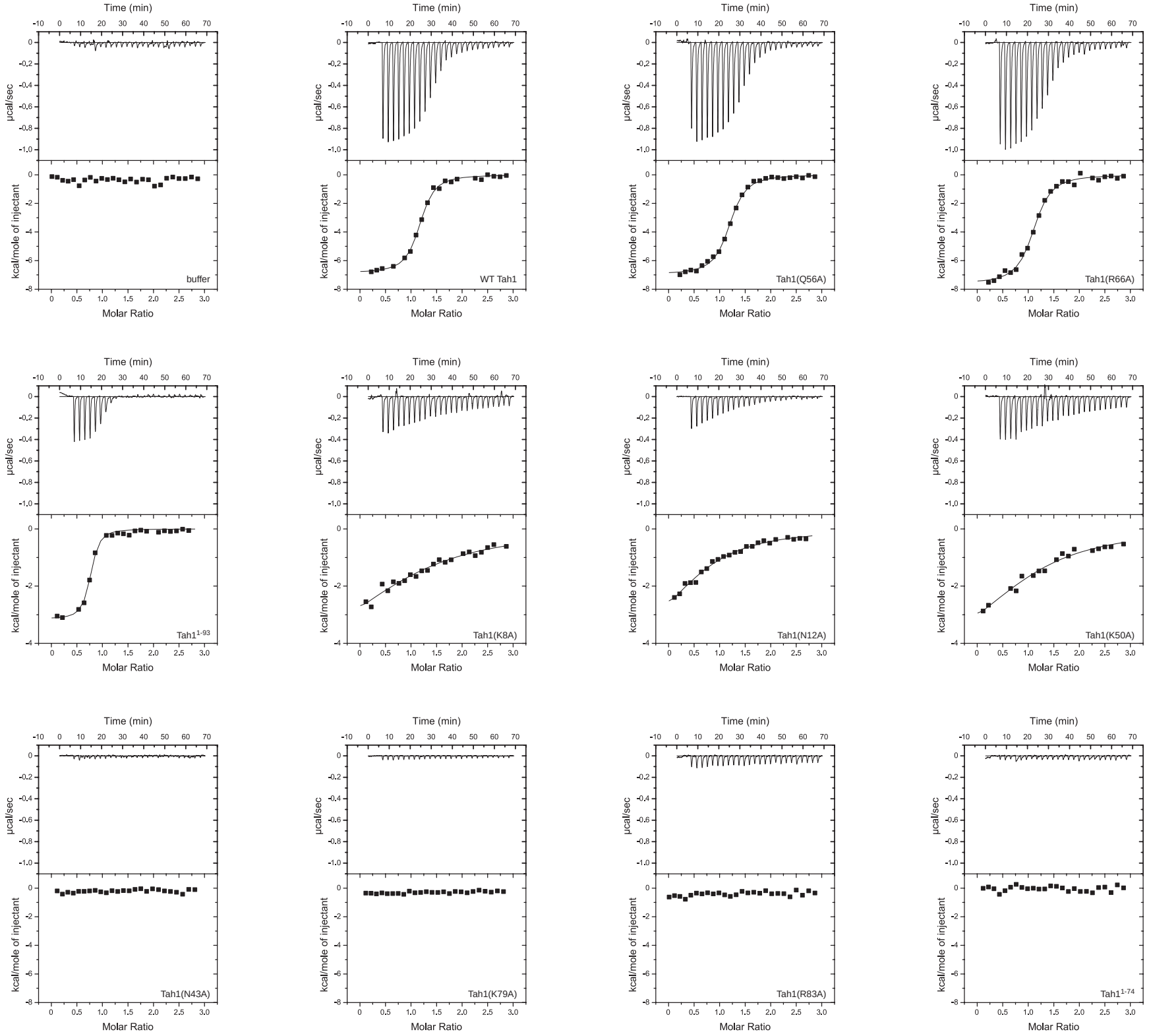
Time (min)
µcal/sec
kcal/mole of injectant
Molar Ratio
buffer
WT Tah1
Tah1(Q56A)
Tah1(R66A)
Tah1(1-93)
Tah1(K8A)
Tah1(N12A)
Tah1(K50A)
Tah1(N43A)
Tah1(K79A)
Tah1(R83A)
Tah1(1-74)

Fig S2